International Journal of Applied Electromagnetics and Mechanics 1 (2018) 1–9
DOI 10.3233/JAE-171047
IOS Press

Finite element method and experimental investigation for hairline crack detection and characterization

Chukwunonso K. Okolo and Turgut Meydan*
Wolfson Centre for Magnetics, School of Engineering, Cardiff University, Cardiff, CF24 3AA, UK

Abstract. This paper reports on a quantitative technique based on the Magnetic Flux Leakage (MFL) method, for the detection and interpretation of the MFL signals caused by rectangular hairline cracks in pipeline structures. This was achieved through visualization and 3D imaging of the leakage field. This research is aimed at detecting hairline cracks caused by granular bond separation, which occurs during manufacturing, leaving pipelines and steel structures with miniature cracks. The investigation compared finite element numerical simulation with experimental data. The response of the MFL probe scanned above a hairline crack was first predicted using an optimized 3D finite element model. The MFL signals associated with both the surface and far-surface cracks were compared. The results show that the depth, width and length of the various hairline cracks can be estimated by using the distribution pattern and strength of the (B_x), (B_y) and (B_z) components of the MFL signals.

Keywords: Defects, finite element modelling, Hall Effect Sensor, magnetic flux leakage, pipeline, steel plate

1. Introduction

Steel pipelines are used to transport oil and gas supplies as part of networks consisting of transmission lines, gathering lines and distribution lines. The operators consistently make use of the in-line Non-destructive testing (NDT) technologies in order to guarantee the integrity and safe operation of these networks. Overtime external forces can impair the pipeline to a state capable of causing a spill or rupture. Cracks and other forms of defects occurring at the surfaces and far-surfaces of in-service pipes, tanks and other industrial components impair their integrity, and can possibly depreciate the service lifetime [1]. Presently, one of the major challenges of the NDT industry is the need to produce an accurate quantitative assessment of the structural integrity of components and assemblies. This is referred to as quantitative non-destructive testing (QNDT). QNDT presents various approaches to detect, estimate and compute the extent of deterioration in terms of the length, width and depth of defects. QNDT also aids in characterizing distinct discontinuities as well as monitoring the life expectancy of materials over a period of time.

The magnetic flux leakage (MFL) technique, which was first carried out on storage tanks in 1988 by Saunderson [2], is a non-contact method of NDT used for locating and characterizing defects both on the surface and far-surface of ferromagnetic steel components. Since the MFL technique can detect both surface and far-surface defects, it is vital to induce a strong enough magnetization field into the wall of the test sample in order to enhance the detection sensitivity and repeatability of the MFL inspection. The MFL technique is direct, easy to implement, highly sensitive, and has been extensively used in the petrochemical, oil and gas industries. Despite the use of so many NDT techniques, the MFL method is

*Corresponding author: T. Meydan, Cardiff University, Newport Rd, Cardiff, UK. E-mail: meydan@cardiff.ac.uk.

commonly considered the cheapest, most frequently used and most effective NDT technique for crack detection and monitoring. It has been used for extremely productive detection of flaws in different types of ferromagnetic components [3], especially in very elongated ferromagnetic structures, such as steel pipes [4,5]. A full MFL signal analysis plan is made up of three processes which are: identification, compensation and characterization [6]. As the MFL pig travels along the pipe, the recorded data will contain a variety of information emanating from various types of defects. The highly hazardous ones are separated from the less hazardous ones using a signal identification procedure. In the compensation stage the leakage signals are compensated for influence of operational variables [7], such as; sensor orientation, lift-off effects, pipe grade, scanning velocity, residual stress, material permeability, etc. The last stage is the defect characterization; the reason for this stage is to ascertain the defects shape and size – an exercise that fall into a wide classification of problems in NDT termed inverse problems. The ability to accurately detect, study and interpret the MFL signals in order to quantify defects is significantly affected by several parameters. Examples of such parameters include; crack orientation, crack geometry (length, width and depth), material permeability, material thickness, magnet system (strength, material, reluctance and lift-off) and sensor system used (type, location and lift-off). The manner in which some of these parameters affect the acquired leakage signal has been investigated by various researchers in the past few years [8–10]. The main objective of this work is to develop an automated direct current MFL (DCMFL) system (i.e. a system that allows for real time data of the scan to be viewed and monitored as the inspection advances, via the LabVIEW user interface) that can effectively detect and quantify hairline surface and far-surface cracks present in ferromagnetic pipeline structures with high accuracy. The investigation compared 3D finite element simulation with practical experiments. The MFL signal associated with both surface and far-surface cracks were compared. Choosing an optimal mesh resolution and proper boundary condition parameters were crucial to ensuring accurate numerical results. The 3D method has proven to be a highly effective tool for modelling the influence of hairline cracks on MFL signals in steel pipelines.

2. Magnetic flux leakage principle

The MFL technique involves magnetizing the test sample, using a permanent or electromagnet, to near or complete saturation. This will generate a magnetic field within the sample. If the wall of the sample is free from any defect, anomalies and imperfections such as, cracks, corrosions, pits, fringes, bends, dents, etc, the generated field will flow through the sample without any obstruction. However, if there are defects within the sample, the magnetic field lines become distorted and a leakage field will be generated at the defective area. This is due to an increase in magnetic reluctance caused by a decrease in magnetic permeability at the defective part [11]. The resulting leakage field can then be measured using an appropriate magnetic field sensor (Hall Effect, AMR or GMR) placed within close proximity of the crack and positioned perpendicular to the direction of the field to be measured. The information obtained from the sensor is used to evaluate the location, shape, size and orientation of the defect. After the inspection is completed, the recorded MFL signals are analyzed and interpreted in terms of the pipeline integrity. Although, the resultant MFL signal corresponds to the crack features, it is still challenging to characterize cracks based on their type and size. Therefore, an in-depth understanding of the shape of the MFL signal is needed so as to establish a more effective defect quantification approach.

3. Finite element computation of MFL numerical models

Previous research has focused on locating the presence of defects that have a direct influence on the integrity of pipelines (large cracks) [12]. However, only limited work has been carried out in terms of the location and evaluation of small imperfections, such as very narrow hairline cracks, especially deep below the surface of pipeline and steel structures. One of the benefits of the Finite element modelling (FEM) is the ability to present a better understanding on how to implement the MFL inspection and to model the leakage field signals from defects. The FEM presents a comprehensive model-prediction of the field pattern in the vicinity of a defect, thus providing a good understanding of the MFL technology.

In this paper, the recent advances in 3D FEM software (MagNet 7.6 software by Infolytica) has been used to model a non-linear system capable of detecting the MFL signals due to hairline cracks [13]. The efficiency of this approach has been assessed for the detection of surface and far-surface cracks in a 10 mm thick carbon steel plate. In order to solve the MFL problem as magnetostatic, the following Maxwell's equations (see Eqs (1), (2) and (3)) have been used with their usual conventional representation and relevant boundary conditions (see Eqs (4) and (5)). Where $\boldsymbol{H}$ is the magnetic field strength, $\boldsymbol{J}_c$ is the current density, $\boldsymbol{D}$ is the electric flux density, $\boldsymbol{B}$ is the magnetic flux density, $\boldsymbol{A}$ is the magnetic vector potential, μ_0 is the permeability of free space, μ_r is the relative permeability of the material used and $\boldsymbol{M}$ is the magnetization of the material used.

$$\nabla \times \boldsymbol{H} = \boldsymbol{J}_c + \frac{\partial \boldsymbol{D}}{\partial t} \tag{1}$$

$$\nabla \cdot \boldsymbol{B} = 0 \tag{2}$$

$$\boldsymbol{B} = \nabla \times \boldsymbol{A} \tag{3}$$

$$\boldsymbol{B} = \mu_0 \mu_r \boldsymbol{H} = \mu \boldsymbol{H} \tag{4}$$

$$\boldsymbol{B} = \mu_0 (\boldsymbol{H} + \boldsymbol{M}). \tag{5}$$

The 3D simulation was solved in the x–y–z plane. A low carbon steel plate with dimension of 350 mm × 60 mm × 10 mm is used for the sample, while a silicon steel material is used for the yoke. The electrical conductivity of the plate and yoke used are 1.32×10^6 S/m and 2.17×10^6 S/m, with a maximum magnetic relative permeability of 100 and 4000 respectively. First, a dc measurement system (electromagnet driven by a quasi dc current by national instrument) was used to obtain the dc hysteresis loop of a typical low carbon steel (test sample) and a silicon steel (yoke) materials. To enable a comparison of the FEM output with the experimental data, BH loops measured for both materials were imported into the MagNet. The yoke was modelled with 300 copper turns, carrying a direct current of 4 A. This generated a magnetic flux density $\boldsymbol{B}$ of 1T in the sample. A hairline crack was inserted at the center of the sample and a measurement distance of 100 mm across the crack was chosen (region with the most uniform flux distribution). All the cracks investigated had a width of 0.2 mm and length of 10 mm. A smaller mesh size of 0.02 mm was used at the inside and outside region of crack as well as on the measurement region in order to achieve accurate results. Boundary conditions has been utilized and set in a region sufficiently larger than the region of interest in order not to affect the result. This setup was used to predict the axial (B_x), radial (B_y), and tangential (B_z), of the MFL signal for both surface and far-surface hairline cracks. The manner in which the magnetization and sensing methodology affects the detection sensitivity of the MFL signal to hairline cracks is investigated. Figure 1a shows the structure of the 3D FEM model used for the simulation, while Fig. 1b shows the B-H characteristic of the low carbon steel sample and silicon steel yoke used. A crack of 0.2 mm width and 0.8 mm depth was used to optimize the magnetization current, and yoke permeability

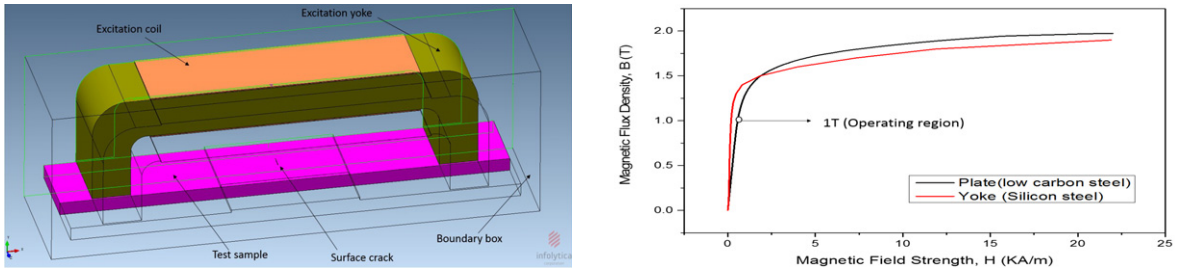

(a) (b)

Fig. 1. Showing (a) FEM schematic layout for the MFL simulation probe alongside crack and (b) Measured B-H curve for the low carbon steel plate and silicon steel yoke imported into the MagNet software.

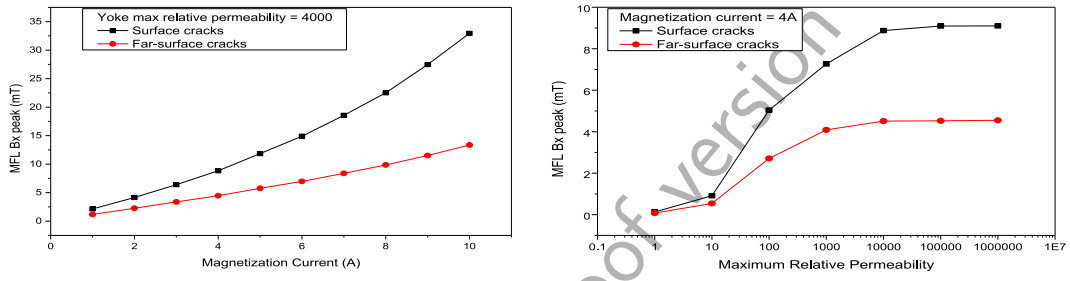

(a) (b)

Fig. 2. Showing (a) the relationship between the (B_x^{peak}) amplitude and magnetization current for a 0.8 mm deep surface and far-surface hairline cracks and (b) the relationship between the MFL (B_x^{peak}) signal amplitude and yoke permeability for a 0.8 mm deep surface and far-surface hairline cracks.

and yoke size. The computational time for the simulation took 25 mins in a dual-core 64-bit processor workstation with 24 GB primary memory.

Figure 2a shows the predicted MFL (B_x^{peak}) signal amplitude at different magnetization currents, for both surface and far-surface hairline crack. The MFL signal has a linear relationship with magnetization current at low current levels and the linearity reduces at higher current levels due to the non-linearity in the B-H curve of the test sample. To avoid saturating the sensor and the need to cool the magnetization coil for longer inspection period, a magnetisation current of 4 A, corresponding to a flux density of 1 T is chosen.

4. Yoke permeability optimization

The amount of flux density generated in the test sample is dependent on the permeability and size of the material used for a given magnet system. However, for most pipeline structures, the material used is low carbon steel which has similar permeability and thickness. Hence the determining factors controlling the amount of flux generated in the test piece is the yoke permeability and size. Therefore the permeability of the material used for the yoke will play a vital role in determining the magnitude of the magnetic flux density ***B*** established within the sample, as well as the amount of leakage field that will occur at the defective part. The higher the permeability of the yoke, the greater the flux density generated in the

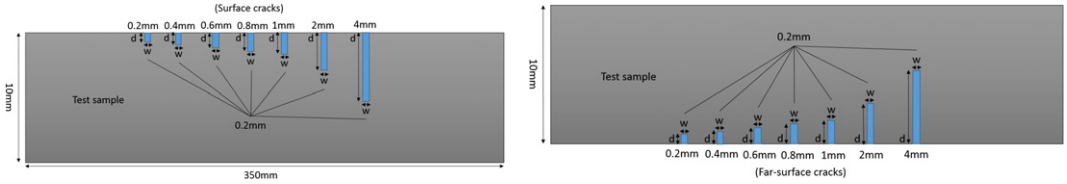

(a) (b)

Fig. 3. Showing a schematic layout of the test sample with (a) surface cracks and (b) far-surface cracks.

sample (before saturation), thus the higher the leakage field B_x that will be measured as shown in Fig. 2b. It can be seen that the magnitude of the MFL (B_x^{peak}) signal increases with increasing maximum relative permeability μ_{rmax} of the yoke, up until a yoke a relative permeability of about 10^4, where the MFL signal becomes constant due to the saturation of the sample. At this point, a further increase in the yoke permeability results in a negligible increase MFL signal amplitude. Hence a yoke maximum relative permeability of 4000 was chosen.

5. Effect of change in crack depth and sensor lift-off

Fourteen different samples with varying surface and far-surface crack depths were used to simulate the effect of change in crack depth on the MFL signal amplitude as shown in Fig. 3. The dimensions of the surface and far-surface hairline cracks used for each sample are specified in Fig. 3a and 3b respectively. Figure 4a shows the relationship between the predicted MFL signal amplitude (B_x^{peak}) and the depth of various hairline cracks with a constant width and length of 0.2 mm and 10 mm respectively. The MFL signal amplitude was found to be strongly related to the crack depth. A small percentage change in crack depth caused a significant change in the (B_x^{peak}) amplitude. Also, the sensor lift-off was varied from 0.5 mm to 10 mm in order to simulate the different levels of sensor lift-off. Figure 4b shows an inverse relationship between the MFL (B_x^{peak}) and the sensor lift-off. The (B_x^{peak}) signal amplitude decreases significantly with increasing sensor lift-off. This shows that lift-off caused by debris and welds during pipeline inspection are capable of causing inaccurate measurements of the true magnitude of the MFL signal which could lead to defects being missed or undersized, especailly for hairline cracks. Also, a greater percentage change in the reduction of (B_x^{peak}) amplitude was observed at lower levels of sensor lift-off when compared to higher levels of sensor lift-off. The MFL field probe showed a good sensitivity up to a lift-off distance of 5 mm.

6. Crack length and width estimation

The typical response of the MFL field probe in the (B_x), (B_y) and (B_z) directions for a 4 mm deep surface hairline crack is displayed in Fig. 5. A method based on visualization and 3D imaging of the resultant leakage signal is proposed in order to obtain the approximate width and length of various hairline cracks present in ferromagnetic pipeline structures. By analyzing the B_x, B_y and B_z signals, it can be seen that the variation of B_y, and B_z leakage signals in the tangential direction, at the edges of the crack is stronger compared to the variation of the B_x leakage signal. Also the B_x field component is a unipolar waveform as shown in Fig. 5a and its signal amplitude is strongly influenced by the crack depth. The B_y field component possess a bipolar sine like waveform with the leakage signal at its minimum along the midpoint of the

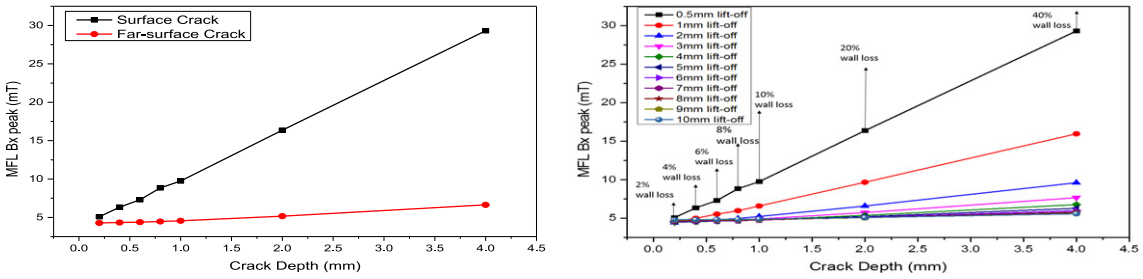

(a) (b)

Fig. 4. Showing (a) the predicted MFL (B_x^{peak}) signal amplitude for both surface and far-surface hairline cracks and (b) comparing the percentage of defect depth to wall thickness at different lift-off values for different surface cracks.

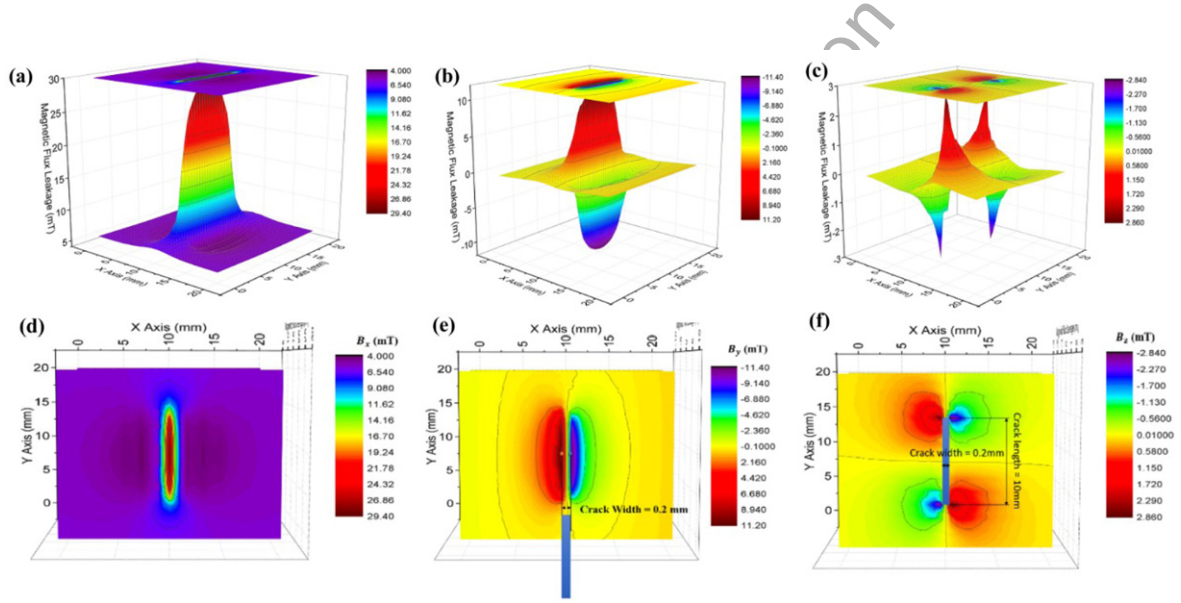

Fig. 5. Showing a 3D illustration of the predicted MFL signal for a 4 mm deep surface hairline crack. (a) B_x component, (b) B_y component, (c) B_z component, (d) Top view of B_x component, (e) Top view of B_y component and (f) Top view of B_z component.

crack (see Fig. 5b). The distance between the peaks and trough highly demonstrates the width of the crack, and the high concentration of flux along the sides of the crack gives a clear indication of the crack location in the x direction mostly around the edges. Also the peaks and trough have an equal amplitude. The B_z field component possess both positive and negative polarities in both the radial and tangential directions (see Fig. 5c) and it highly demonstrates both the width and length of the crack. The high concentration of leakage flux around the crack edges also gives in indication of the crack position. Hence the shape and approximate size of the crack could be obtained from the distribution patterns of B_y and B_z signals. Figure 5d, 5e and 5f shows the signal patterns with respect to the sensing path distance. The width and length sizes of the crack can be obtained from the width of the crack signal along the width and length directions respectively as displayed in Fig. 5e and 5f.

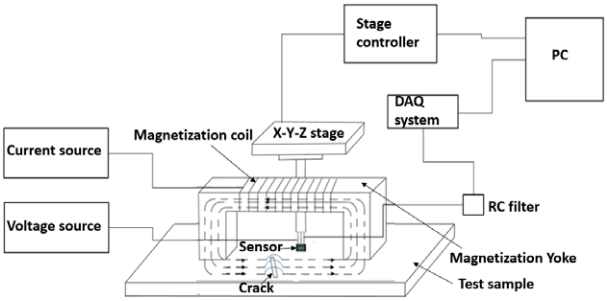

Fig. 6. Showing the DCMFL experimental probe system set-up.

7. Experimental method

The experimental setup used for the investigation is shown in Fig. 6. The low carbon steel samples used have both surface and far-surface hairline cracks, positioned perpendicular to the field orientation. The cracks were artificially fabricated by electrical discharge machining (EDM). The magnetization characteristic curve for the silicon steel yoke and low carbon steel samples inspected is shown in Fig. 1b. The measured saturation magnetic flux density for the low carbon steel sample used is 1.8 T. A non-defective sample was first magnetized with a direct current of 4 A, and 20 turns of copper wire with a diameter of 0.2 mm was wound around the center of the sample. The copper wire was connected to a flux meter and a corresponding magnetic flux density of 1.04 T was read off the flux meter. The depth of the cracks used ranges from 0.2 mm to 4 mm with a constant width and length of 0.2 mm and 10 mm respectively, representing both mild and severe cases of naturally occurring cracks in pipeline structures. Measurements were made by scanning a single Hall Effect sensor (A1302KUA-T) with a sensitivity of 1.377 mV/G across the center of the cracks, with a constant scan step size and sensor lift-off of 0.5 mm and 0.5 mm respectively. An X-Y-Z translation stage was used to move the sensor along the sample surface. The sensor was held in place by a 3D printed sensor holder and positioned perpendicular to the field orientation to measure the axial B_x component of the leakage signal at each scan step. The sensor output is filtered by a low-pass filter with a cut-off frequency of 10 Hz and the filtered output is digitized by a data acquisition system (NI USB-6366) with 16-bit analogue to digital conversion card and then stored in a computer for signal processing. Data were collected at 1000 samples/sec for each scanning cycle.

8. Experimental results and discussion

A range of surface and far-surface crack depths were investigated. Figure 7a and 7b show the measured (B_x) component of the leakage field with respect to the axial scanning distance, for the surface and far-surface hairline cracks respectively. As can be seen, the B_x amplitude increases with increase in crack depth. The MFL system is able to detect a 0.2 mm deep (2% wall loss) surface crack and a 0.6 mm deep (6% wall loss) far-surface crack located 9.4 mm below the sample surface. However the system is not able to detect a 0.2 mm and 0.4 mm deep far-surface crack located 9.8 mm and 9.6 mm below the sample surface respectively. Figure 8a and 8b shows a 3D map representing the typical axial leakage field component (B_x) obtained at the vicinity of a 4 mm deep surface and 4 mm deep far-surface hairline cracks respectively, as a function of x and y displacements. As the tangential cracks are detected, the amplitude and distribution patterns of the leakage fields are altered with respect to the shape of the cracks. The

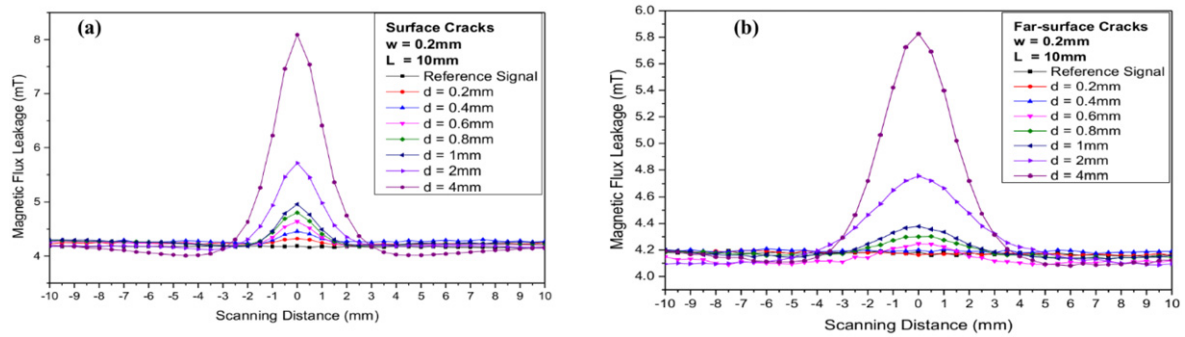

Fig. 7. Showing the measured MFL signals (B_x) as a function of crack position for; (a) Surface cracks and (b) Far-surface cracks.

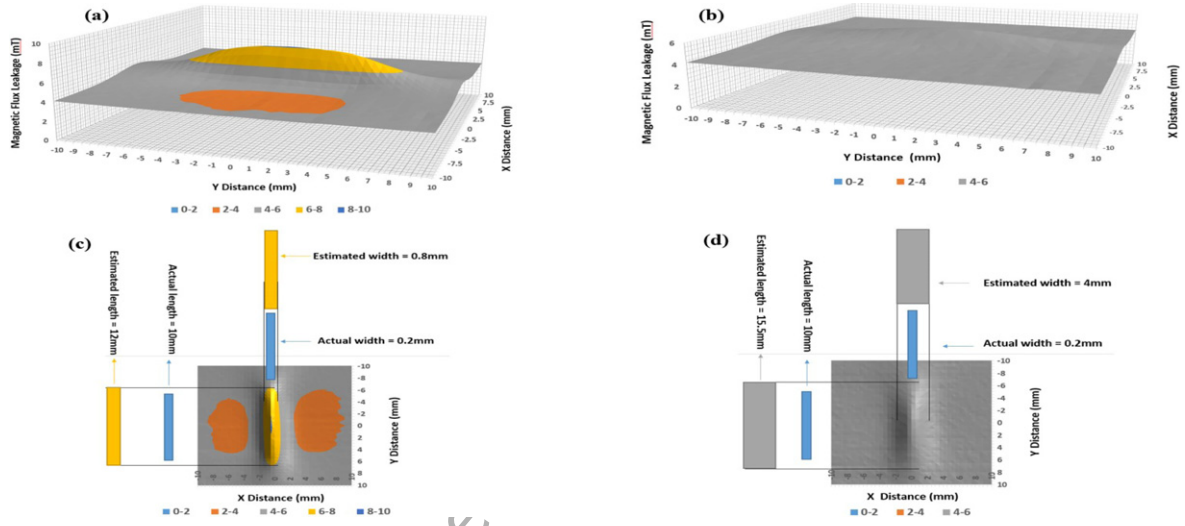

Fig. 8. Showing the measured B_x component of the leakage field for; (a) 4 mm deep surface crack, (b) 4 mm deep far-surface crack: top view of the B_x component of the leakage field for; (c) 4 mm deep surface crack and (d) 4 mm deep far-surface crack.

relationship between the shape of the cracks and the resultant leakage signal could be established by analyzing the distribution change of the flux. Figure 8c and 8d show the leakage field distribution pattern with respect to the sensing path distance for both the surface and far-surface cracks. The width and length of both cracks can be estimated by analyzing the leakage field pattern in the width and length directions respectively. An approximate length of 12 mm and 15.5 mm was estimated for the surface and far-surface cracks respectively, and an approximate width of 0.8 mm and 4 mm respectively. The broader signal profile observed for the far-surface crack when compared to a surface crack of the same size is attributed to the lateral spread of magnetic field at the far-surface crack region.

9. Conclusions

In this paper, the amount of leakage flux needed to accurately detect hairline surface and far-surface cracks was established. A 3D FEM model was used to optimize the magnetization and sensing methodology in order to improve the detection sensitivity of the MFL technique. Experimental data was found

to have a good correlation with the predicted results. The optimized MFL system was able to estimate the actual width and length of the surface and far-surface cracks investigated, by analyzing the leakage field pattern in the width and length directions respectively. The experimental system was able to capture a 0.2 mm deep (2% wall loss) surface crack and a 0.6 mm deep (6% wall loss) far-surface crack positioned 9.4 mm below the sample surface. However the system is not able to detect a 0.2 mm and 0.4 mm deep far-surface crack located 9.8 mm and 9.6 mm below the sample surface respectively. The MFL peak was found to be strongly determined by the crack depth, a slight variation in depth causes a significant change in the MFL peak value. The MFL sensor maintained a good sensitivity to a 4 mm deep surface and 4 mm deep far-surface cracks at lift-off distance of 5 mm. This makes the developed MFL system very useful for applications where large lift-off values are required between the sensor and the measurement surface. Also the simulation results show that analyzing the B_y and B_z leakage field components can yield additional information about the leakage field distribution due to various hairline cracks, which can be used to quantify the cracks based on their length and width sizes. Future work will look at obtaining the B_y and B_z leakage field distribution using practical experiment, which will significantly improve the hairline crack quantification of the developed MFL system. In conclusion, an optimized MFL system that can effectively detect and characterize hairline cracks existing in elongated pipeline networks has been developed for hairline crack detection and quantification.

References

[1] J. Wilson and G.Y. Tian, Pulsed electromagnetic methods for defect detection and characterisation, *NDT&E International* **40** (2007), 275–283.

[2] D.H. Saunderson, The MFE tank floor scanner – a case history, *IEEE Colloquium on Non-Destructive Evaluation* (1988).

[3] J. Wu, Y. Sun, Y. Kang and Y. Yang, Theoretical analyses of MFL signal affected by discontinuity orientation and sensor-scanning direction, *IEEE Trans. Magn.* **51** (2015), 1–7.

[4] J. Drury, *Magnetic Flux Leakage Technology*, Silverwing (UK) Ltd, 2012, [Online], Available at: http://www.silverwingndt.com. [Accessed 5 December 13].

[5] W. Jianbo, F. Hui, W. Jie and K. Yihua, The influence of non-uniform wall thickness on MFL testing for a steel pipe, *Insight* **57** (2015), 703–708.

[6] L. Udpa, S. Mandayam, S. Udpa, W. Lord and Y. Sun, Magnetic flux leakage inspection of gas pipelines: Neural networks for signal characterization, compensation and identification (Topical Report: GRI-96), tech. rep., *Gas Research Institute*, Chicago, IL, 1996.

[7] W.L. Mandayam, L. Udpa and S. Udpa, Wavelet-based permeability compensation technique for characterizing magnetic flux leakage images, *NDT&E International* **30**(5) (1997), 297–303.

[8] Y. Kang, J. Wu and Y. Sun, The use of magnetic flux leakage testing method and apparatus for steel pipe, *Mater. Eval.* **70** (2012), 821–827.

[9] M. Katoh et al., Modelling of the yoke-magnetization in MFL-testing by finite elements, *NDT & International* **36**(7) (2003), 479–486.

[10] M. Katoh, K. Nishio and T. Yamaguchi, FEM study on the influence of air gap and specimen thickness on the detectability of flaw in the yoke method, *NDT & International* **33**(5) (2000), 333–339.

[11] S. Yan et al., Theory and application of magnetic flux leakage pipeline detection, *Sensors* **15**(12) (2015), 31036–31055.

[12] F.I. Al-Naemi, J.P. Hall and A.J. Moses, FEM modelling techniques of magnetic flux leakage-type NDT for ferromagnetic plate inspection, *Journal of Magnetism and Magnetic Materials* **304**(2) (2006), 790–793.

[13] T. Ide and M. Okada, Numerical simulation for a nonlinear partial differential equation with variable coefficients by means of discrete variational derivative method, *Journal of Computational and Applied Mathematics* **194**(2) (2006), 425–459.